Growth of Wrinkle-Free Graphene on Texture-Controlled Platinum Films and Thermal-Assisted Transfer of Large-Scale Patterned Graphene

Jae-Kyung Choi,[†] Jinsung Kwak,[†] Soon-Dong Park,[‡] Hyung Duk Yun,[†] Se-Yang Kim,[†] Minbok Jung,[†] Sung Youb Kim,[‡] Kibog Park,[§] Seoktae Kang,[∥] Sung-Dae Kim,[⊥] Dong-Yeon Park,[#] Dong-Su Lee,[#] Suk-Kyoung Hong,[#] Hyung-Joon Shin,[*,†] and Soon-Yong Kwon[*,†,‡]

[†]School of Materials Science and Engineering, Ulsan National Institute of Science and Technology (UNIST), Ulsan 689-798, Korea, [‡]School of Mechanical and Nuclear Engineering, Ulsan National Institute of Science and Technology (UNIST), Ulsan 689-798, Korea, [§]Department of Physics, Ulsan National Institute of Science and Technology (UNIST), Ulsan 689-798, Korea, [∥]Department of Civil Engineering, Kyung Hee University, Gyeonggi 446-701, Korea, [⊥]Advanced Characterization and Analysis Group, Korea Institute of Materials Science, Changwon 642-831, Republic of Korea, and [#]GMEK Incorporation, Gyeonggi 431-767, Korea

ABSTRACT Growth of large-scale patterned, wrinkle-free graphene and the gentle transfer technique without further damage are most important requirements for the practical use of graphene. Here we report the growth of wrinkle-free, strictly uniform monolayer graphene films by chemical vapor deposition on a platinum (Pt) substrate with texture-controlled giant grains and the thermal-assisted transfer of large-scale patterned graphene onto arbitrary substrates. The designed Pt surfaces with limited numbers of grain boundaries and improved surface perfectness as well as small thermal expansion coefficient difference to graphene provide a venue for uniform growth of monolayer graphene with wrinkle-free characteristic. The thermal-assisted transfer technique allows the complete transfer of large-scale patterned graphene films onto arbitrary substrates without any ripples, tears, or folds. The transferred graphene shows high crystalline quality with an average carrier mobility of ~5500 $cm^2 V^{-1} s^{-1}$ at room temperature. Furthermore, this transfer technique shows a high tolerance to variations in types and morphologies of underlying substrates.

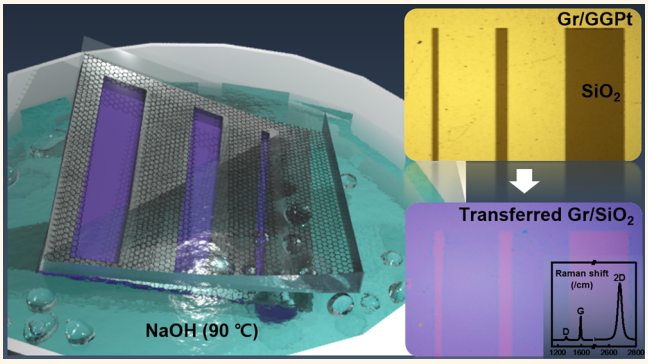

KEYWORDS: wrinkle-free graphene · patterned graphene · thermal-assisted transfer · chemical vapor deposition · texture-controlled platinum

Graphene, a two-dimensional material composed of a monolayer of carbon (C) atoms, has generated enormous scientific curiosity owing to its ultrathin geometry and unique characteristics.[1−4] The first successful isolation of graphene was achieved by micromechanical cleavage from graphite; however, the sizes of graphene flakes are too small for practical applications.[1] To overcome this limitation, several experimental methods including surface graphitization of SiC,[5,6] solid source deposition,[7,8] and chemical vapor deposition (CVD)[9−12] have been explored for large-scale graphene formation. Among these, CVD of hydrocarbon gases has been demonstrated as an attractive approach because of the ability to grow high-quality graphene films over large areas and wide accessibility of industrial equipment. However, special care should be taken to precisely control the thickness and uniformity of the resulting graphene layers in CVD process, since the growth kinetics of graphene is complicated by the growth parameters such as growth temperature, pressure, cooling rate, and solubility of C atoms in catalytic metal substrates, *etc.*[9−12] All of these factors contribute to the thickness and structural homogeneity of graphene over large areas.

At present, monolayer graphene films are best synthesized via pyrolytic cracking

* Address correspondence to sykwon@unist.ac.kr, shinhj@unist.ac.kr.

Received for review October 25, 2014 and accepted December 15, 2014.

Published online December 15, 2014
10.1021/nn5060909

of hydrocarbon gases at elevated temperatures (~1000 °C) onto polycrystalline copper (Cu) surfaces and later transferred to other substrates for the fabrication of devices.[10] Since Cu has a very low solubility of C atoms (<0.004% at 1000 °C),[13] the nonequilibrium precipitation is not significant in the CVD growth of graphene on Cu, which primarily leads to the formation of monolayer graphene films. In particular, CVD growth on Cu foils has recently attracted significant attention due to its great potential for the growth of large domain, single crystalline graphene by simply controlling growth parameters during CVD process.[14−16] However, the high growth temperatures impose limitations on the crystalline quality of the resulting films because of the large thermal expansion coefficient (TEC) difference of Cu to graphene, which causes the formation of high density of crystalline defects such as wrinkles in the obtained graphene layers.[17]

For these reasons, significant efforts have recently been directed toward the rational design of catalytic metal substrates as well as development of novel transfer processes that provide direct access to defect-free, homogeneous monolayer graphene films. The suitable metallic substrates with small TEC difference to graphene will facilitate the formation of defect-free graphene films. Platinum (Pt) is one of most commonly used materials for the bottom electrodes as it exhibits excellent properties in thermal stability and chemical resistance. Besides, the smaller TEC difference of Pt (~11 μm m^{-1} K^{-1})[18,19] to graphene (~6.7 μm m^{-1} K^{-1}),[20] compared to other conventional metallic substrates for graphene growth such as Cu (~21 μm m^{-1} K^{-1})[21,22] or Ni (~17 μm m^{-1} K^{-1}),[23,24] is believed to contribute to far less defects formation in the resulting graphene layers. In contrast to Cu, Pt has relatively high C solubility of ~0.9 atom % at 1000 °C.[21,25] As a result, the dissolution of C atoms into metal and the subsequent nonequilibrium precipitation process generally lead to the inhomogeneous graphene growth after high-temperature CVD growth. Another problem of graphene grown on noble metals is that we cannot transfer graphene using the currently used etching-based processes. Very recently, Wang *et al.*[26] have demonstrated a nondestructive electrochemical route for delamination of graphene from Cu surface and an electric bubbling transfer method has been proposed regarding the transfer of graphene grown on novel metallic surfaces such as Pt to the target substrates.[27] Considering the principle of the electric bubbling transfer method, however, it will be difficult to apply this method when the graphene films are formed on the patterned Pt or Pt substrates including insulator regions such as SiO_2. Evidently, the growth of large-scale patterned, wrinkle-free graphene and the gentle transfer technique without further damage are most important requirements for the practical use of graphene in various applications.

Here, we report an alternative strategy for the CVD growth of strictly monolayer, wrinkle-free graphene films using a texture-controlled Pt substrate and a thermal-assisted transfer technique to transfer the graphene without any further defect formation in a NaOH aqueous solution. Our key strategy is to utilize the Pt substrates with textured, *i.e.*, preferred orientation-controlled giant grain to limit number of grain boundaries (GBs) of polycrystalline Pt surface, which is believed to be the origin of inhomogeneous graphene growth.[9,11,28] Improving the surface perfectness of the Pt substrates by increasing the size of grains up to millimeter scale would be of immense benefit to the production of well-crystallized graphene structure. Moreover, the highly oriented single crystalline Pt film offers more atomically flat and smooth surfaces and the use of Pt as an underlying catalytic surface results in the wrinkle-free graphene layers. As a result, the formation of strictly monolayer, wrinkle-free graphene on Pt has been achieved successfully, even on the high C-soluble metallic material, Pt. More importantly, our thermal-assisted transfer technique enables us to transfer large-scale patterned graphene films onto arbitrary substrates without any wrinkles/ripples formation, which is also applicable to other metallic substrates such as Cu. Consequently, our wrinkles/ripples-free graphene films transferred on SiO_2/Si substrates showed a high crystalline quality with an average room-temperature carrier mobility of ~5,500 cm^2 V^{-1} s^{-1}. We believe that our approach may promote the current efforts of graphene applications.

RESULT AND DISCUSSION

Texture-Controlled Giant Grain Growth of Platinum Thin Films. The 400 nm-thick Pt films were deposited at room temperature on SiO_2/Si substrates by direct current magnetron sputtering. Typical sputtering power, growth time, and gas pressure were ~170 W, 30 min, and ~9.4 mTorr, respectively. Pt films are usually (111)-oriented since (111) planes are ones with lowest surface energy.[29] It was reported that the preferred orientation of Pt thin films on SiO_2/Si substrates could be controlled by sputtering with Ar/O_2 gas mixtures and was affected by the incorporation of oxygen in the Pt films.[29,30] In this study, the texture of as-deposited Pt films was changed from (111) to (200) orientation by increasing the oxygen fraction to 5% in the sputtering gas mixture of Ar/O_2 gas. We further observed the changes in preferred orientation of Pt films to (220) orientation when the pressure was decreased to ~7.8 mTorr during Pt sputtering. It is believed that the surface mobility of Pt adatoms decreased with oxygen adsorption, and consequently (200) and (220) planes developed instead of (111) planes, *i.e.*, the energetically most stable planes.[31−34] The postannealing process was performed at ~1000 °C

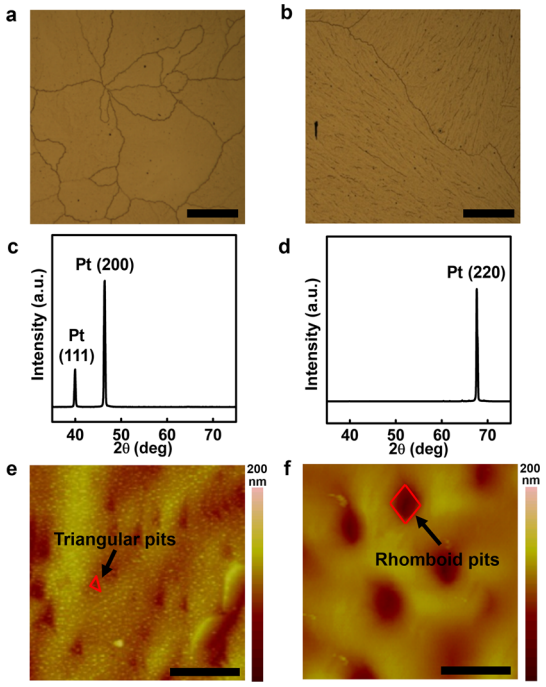

Figure 1. Surface morphologies and crystallographic orientations of Pt films with texture-controlled giant grains. (a and b) Optical microscopy images of (a) Pt(200)- and (b) Pt(220)-oriented films with giant grains (scale bars: 200 μm), (c and d) XRD patterns of (c) Pt(200)- and (d) Pt(220)-oriented films with giant grains, (e and f) AFM images of unintentionally etched (e) Pt(200)- and (f) Pt(220)-oriented films with giant grains (Scale bars: 2 μm).

for 60 min in ambient air to remove the incorporated oxygen and to observe the giant grain growth behaviors of Pt films. The dramatic changes in surface morphologies and preferred orientations of the Pt films were observed by optical microscopy (OM), X-ray diffraction (XRD) and atomic force microscopy (AFM), as shown in Figure 1. The Pt films completely transformed to giant grains with sizes as large as several hundreds of micrometers to a millimeter, as observed by OM images in Figure 1a-1b. Furthermore, the preferred orientation of the giant grains could be controlled to have either (200) or (220) textures (Figure 1c, d). For the films with (200) preferred orientation, they had a small portion of (111) orientation, as observed in the XRD pattern. Previous studies have shown that the incorporated oxygen was driven out by decomposition of platinum oxide phases when the sputtered films were annealed and the giant grain growth process occurred.[29−32,34] The crystallinities of the giant grains were confirmed by observing the unintentionally etched surfaces of the Pt films using an AFM, as shown in Figure 1e-1f. The shapes of etch pits are identical, *i.e.* triangular or rhomboid pits from (200) or (220) giant grains, respectively, implying that the giant grain is a single crystal.

Growth of Wrinkle-Free, Monolayer Graphene Films on Texture-Controlled Pt Films with Giant Grains. Figure 2 shows the representative surface morphologies of the

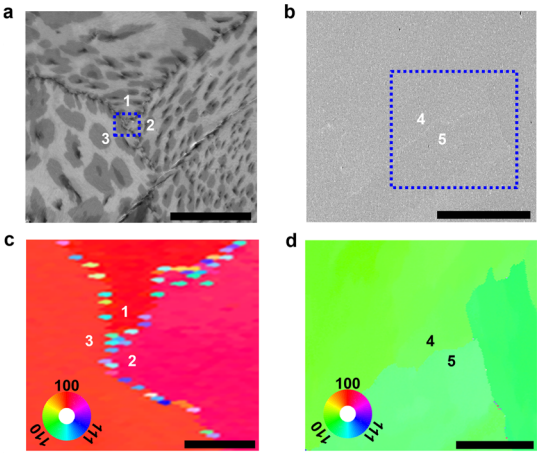

Figure 2. Structural characterization of graphene films grown on GGPt films with different preferred orientations. (a and b) Representative SEM images of monolayer graphene grown on (a) GGPt(200) and (b) GGPt(220) surfaces (scale bars: 100 μm). Dark gray islands in (a) indicate the presence of few-layer graphene flakes on monolayer graphene films. (c and d) corresponding EBSD map images obtained from the regions highlighted by the dotted rectangles in (a and b) (scale bars: 10 μm (left), 50 μm (right)).

graphene layers that were grown on Pt(200)- and Pt(220)-oriented films with giant grains (*i.e.*, GGPt(200) and GGPt(220), respectively). After the GGPt films were loaded into a quartz tube, each sample was heated to the process temperature of ~975 °C and maintained for 10 min under CH_4/H_2 gas mixture (5 and 50 sccm, respectively). After graphene growth, the tube was cooled down to room temperature naturally. In all our growth experiments, the monolayer graphene layers were formed over large areas regardless of the types of the underlying surfaces. However, the monolayer graphene grown on GGPt(200) contains a high density of few-layer graphene (FLG) flakes (Figure 2a), in contrast to the strictly uniform, monolayer graphene films that achieved on GGPt(220) (Figure 2b). Interestingly, the presence of FLG flakes is observed on the surfaces of etch pits and along the GBs of GGPt(200) surfaces, implying that such defects function as the main segregation channels of C atoms. From the electron backscatter diffraction (EBSD) map, we have found that the sizes and densities of the overgrown FLG flakes at the each region (from 1 to 3 in Figure 2c) depend on the orientation of underlying Pt surfaces. The closer Pt orients to the (111) plane, the smaller the diameter and the greater the density of the FLG flakes, suggesting that growth kinetics of graphene is sensitive to the orientation of underlying Pt surfaces.[35] This result is typical of several tens of SEM and EBSD images of graphene/GGPt(200) acquired from different regions. We note that all of the graphene area on GGPt(220) had a single layer and no FLG was observed. Apparently, there existed a remarkable improvement in the structural homogeneity of graphene on the

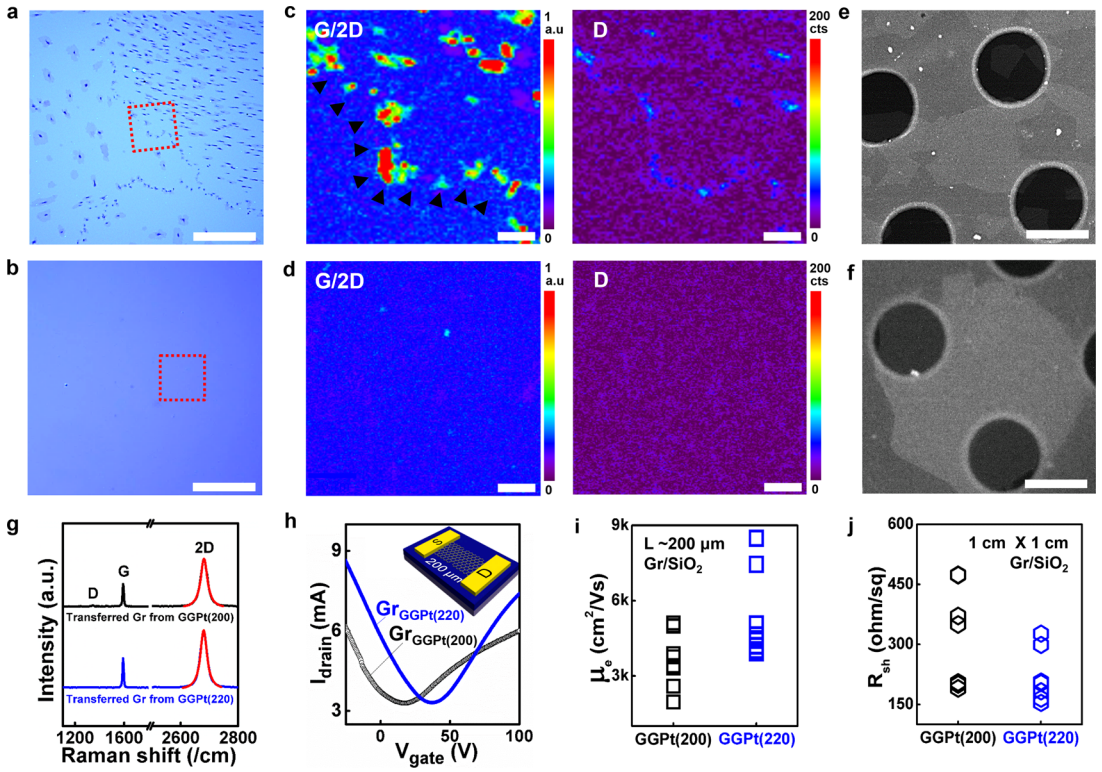

Figure 3. Structural and electrical characterizations of transferred graphene films onto SiO_2 surfaces. (a and b) Optical microscopy images of graphene films grown on (a) GGPt(200) and (b) GGPt(220) films then transferred to SiO_2/Si substrate (scale bars: 50 μm), (c and d) Corresponding Raman map images of the G/2D bands and D band of graphene obtained from the regions highlighted by the dotted rectangles in (a and b) (Scale bars: 5 μm), (e-f) TEM images of graphene films grown on (e) GGPt(200) and (f) GGPt(220) films then transferred to holey carbon film coated Au grids (scale bars: 1 μm), proving the wrinkle-free characteristic of the resulting films, (g) representative Raman spectra of graphene films grown on (top) GGPt(200) and (bottom) GGPt(220) films then transferred to SiO_2/Si substrate, (h) typical room temperature $I_{DS}-V_G$ curves at V_{DS} = 5 V from the transferred graphene-based back-gated FET devices. Inset shows the schematic illustration of the FET devices used in this study. The estimated carrier mobilities of graphene grown on GGPt(200) (black dotted line) and GGPt(220) (blue line) are ~3734 and ~5479 cm^2V^{-1} s^{-1} at room temperature, respectively. (I and j) (i) The estimated room-temperature carrier mobilities and (j) sheet resistances of transferred graphene films.

GGPt(220) surfaces compared with the graphene/GGPt(200) surfaces. It is likely that the single crystalline, atomically flat GGPt(220) surface with a smaller lattice constant difference to graphene (~-6.2%), compared to other crystallographic orientations of Pt such as (111) (~12.6%), (200) (~29.9%) (Supporting Information Figure S1) provides an initial venue for uniform growth of monolayer graphene. Moreover, it is worth noting that the as-synthesized monolayer graphene films were wrinkle-free and smooth over large areas, regardless of the orientations of the underlying Pt surfaces, in contrast to the graphene grown on Cu (Supporting Information Figure S2). We believe that the wrinkle-free graphene growth is favored by the relatively small TEC difference of Pt to graphene.

We have further examined the structural properties of transferred graphene films using OM and Raman spectroscopy. For graphene grown on the GGPt films, we have developed a thermal-assisted transfer technique based on a NaOH aqueous solution and the detailed transfer process will be explained later. Figure 3a and 3b shows the OM images of graphene films grown at ~975 °C for 10 min on the GGPt(200) and GGPt(220), respectively, then transferred onto SiO_2 surfaces. We note that the transferred graphene films perfectly preserve their original morphological features. For the transferred graphene that was grown on the GGPt(200), the presence of FLG flakes especially along the surface pits and GBs of the underlying Pt is clearly illustrated in the Raman map images of G/2D and D bands, as shown in Figure 3c. Meanwhile, in the case of the transferred graphene that was grown on the GGPt(220), the ratio of G-to-2D intensity is less than 0.5 and the intensity of D band is quite low, in all investigated areas (Figure 3d), revealing that almost defect-free monolayer graphene was formed. We note that the transferred graphene films were free from wrinkle-characteristic (Figure 3e-3f). Furthermore, the Raman 2D bands, which were collected over 100 different points on the transferred graphene, exhibits a symmetric single Lorentzian line shape with a full-width at half-maximum of ~31 cm^{-1} (Figure 3g), proving the formation of strictly uniform, monolayer graphene films.[7−12]

The electrical properties of transferred graphene layers that were grown on the GGPt(200) and

GGPt(220) surfaces have been evaluated with back-gated field effect transistor (FET) devices and typical data for the FET devices are shown in Figure 3h. FET devices with a channel length of 200 μm and a channel width of 100 μm atop 300 nm SiO_2 with a p-Si back gate were fabricated by the conventional photolithography. All of the reported electrical measurements were taken at room temperature in air and more details can be found in Experimental Section. The ambipolar transport characteristics and the shift of neutrality point to positive gate voltage are observed for all of the samples, which are characteristics of pristine graphene.[1] As exhibited by the Raman measurements, the electrical properties of the strictly uniform, monolayer graphene grown on GGPt(220) were superior to those of graphene grown on GGPt(200). For example, the average room-temperature carrier mobility of the graphene grown on GGPt(220) is ~5500 $cm^2 V^{-1} s^{-1}$, which is ~1.5 times larger than that of the graphene grown on GGPt(200) (Figure 3i). This mobility is larger than, or comparable to, those of graphene on SiO_2 surface recently reported in the literatures[9−12,14−16,27] and this high value is believed to be originated from high crystalline quality of the wrinkle-free graphene grown on GGPt and transferred by a thermal-assisted transfer. In addition, the average sheet resistances of transferred graphene layers (with sizes of ~1 cm^2) that were grown on GGPt(220) and GGPt(200) surfaces, measured using the van der Pauw method, were found to be ~200 and ~350 Ω per square, respectively (Figure 3j).

Thermal-Assisted Transfer of Large-Scale Patterned Graphene from Pt Substrates. One of the most fascinating features of the presented approach is its high tolerance to variations in types and morphologies of underlying substrates during transfer process. The thermal-assisted transfer process is nondestructive and allows the complete transfer of large-scale patterned graphene films onto arbitrary substrates without any wrinkles/ripples formation (Supporting Informarion Figures S3−S4). Furthermore, it can be applicable to the conventional metallic substrates such as Cu foils or films; however, the Cu was partially oxidized due to its high chemical reactivity with the electrolyte, similar to the reported electric bubbling transfer process.[27] The detailed process of the thermal-assisted transfer is as follows (Figure 4a): After CVD growth, a layer of poly(methyl methacrylate) (PMMA) was spin-coated onto the graphene grown Pt substrates. Then the PMMA/graphene/Pt was floated on a NaOH (1 M) aqueous solution at ~90 °C, and the PMMA/graphene layer was spontaneously separated from the Pt surface after 60 min. After being rinsed DI water for 30 min, the PMMA/graphene layer was transferred onto the target surface. Then the sample was dried on a hot plate at ~40 °C for 30 min, and ~105 °C for 10 min. Finally, the PMMA was removed by washing with acetone. In the

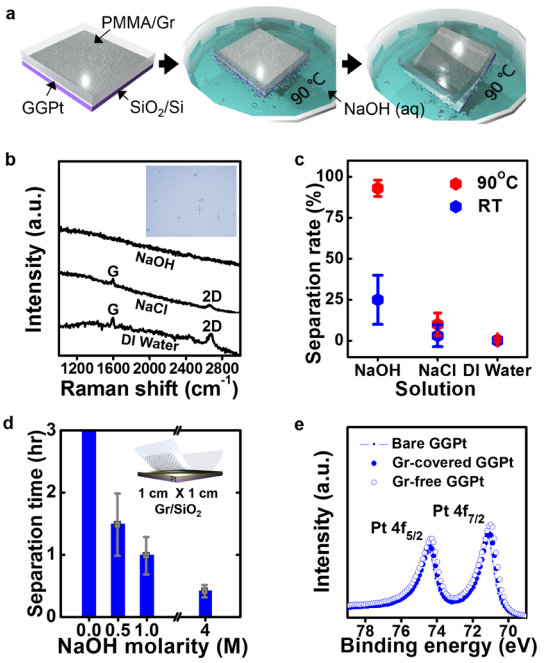

Figure 4. Thermal-assisted transfer process of graphene from a Pt surface. (a) Schematic illustration of the thermal-assisted transfer process. (b) Raman spectra from graphene/Pt films after the thermal-assisted transfer process in various boiling solutions (90 °C) of NaOH (top), NaCl (middle), and DI water (bottom). Inset shows OM image of graphene-free surface of Pt after the transfer process in NaOH, (c) Plot of a success rate of graphene transfer from a Pt surface in various solution at room temperature and 90 °C. (d) Changes in the separation time of graphene from a Pt surface under various NaOH molarities. (e) High-resolution Pt-4f XPS spectra of bare GGPt, graphene-covered GGPt, and graphene-free surfaces after the thermal-assisted transfer process.

thermal-assisted transfer process, we note that it was not possible to separate the PMMA/graphene layer from the Pt surface using boiling solutions other than the NaOH, such as NaCl or deionized (DI) water (Figure 4b-4c), suggesting that the hydroxide (OH^-) in boiling NaOH solution is responsible for the reaction at the graphene/Pt interface. Generally, metals are known to be attacked in a NaOH solution by forming metal hydroxide (*e.g.*, platinum hydroxide) at temperatures higher than 300 °C[36,37] however, the temperature used in our transfer method (90 °C) was considerably lower than 300 °C. This resulted in much slower detachment of graphene from the Pt surface than the electric bubble transfer method,[27] however, allowed the complete transfer of graphene films without any tears and/or folds. In the same vein, the separation time of the PMMA/graphene from the Pt surface strongly depends on the molarities of NaOH solutions, as shown in Figure 4d. By increasing the molarity of an NaOH solution from 0.5 to 4 M, the separation time was reduced from ~90 to ~30 min and it was saturated to 30 min with molarities of NaOH over 4 M. Notably, our transfer method was absent of unintentional contamination on Pt surfaces during

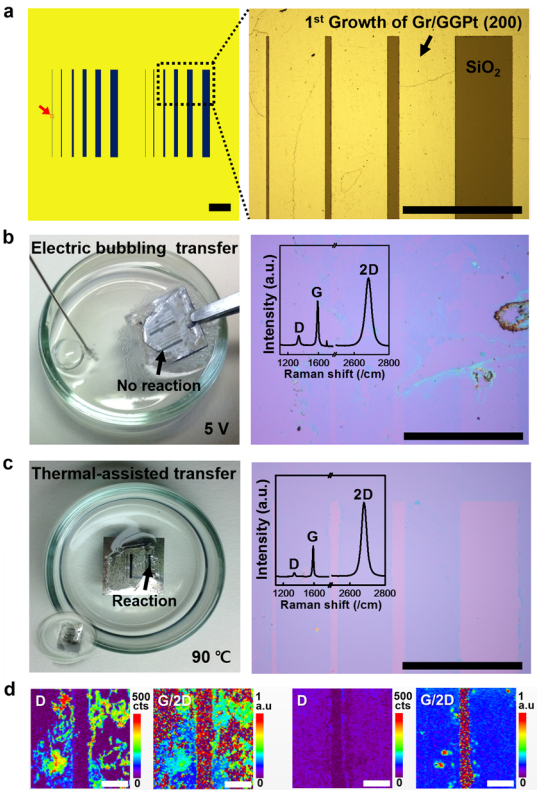

Figure 5. Complete transfer of graphene grown on a patterned GGPt substrate using the thermal-assisted transfer technique. (a) Schematic illustration of a GGPt film with various geometries (left) and an OM image of graphene grown on a patterned GGPt surface after CVD growth (right). (b) A photograph showing the graphene transfer process from a patterned GGPt surface using an electric bubbling transfer technique (5 V, 25 °C) (left) and a representative OM image of the resulting patterned graphene sheet transferred onto SiO_2 surface after the removal of PMMA layer (right). (c) A photograph showing the graphene transfer process from a patterned GGPt surface using a thermal-assisted transfer technique (1 M NaOH, 90 °C) (left) and a representative OM image of the resulting patterned graphene sheet transferred onto SiO_2 surface after the removal of PMMA layer (right). The scale bars of all images in (a)−(c) are 1 mm. (d) Raman maps of the D band and the G/2D band of the patterned graphene sheet transferred onto SiO_2 surface by an electric bubbling transfer (left) and by a thermal-assisted transfer (right) techniques (scale bars, 10 μm). The red arrow in (a) denotes the same location in the Raman mapping images.

transfer process. Figure 4e shows the Pt-4f XPS spectra taken on the samples of bare GGPt, graphene-covered GGPt, and graphene-free GGPt after the thermal-assisted transfer process. All the spectra revealed the Pt-$4f_{5/2}$ peaks at the same binding energy of 74 ± 0.2 eV and almost insignificant changes in the relative intensities of the Pt-$4f_{5/2}$ and Pt-$4f_{7/2}$ peaks were observed, indicating no contamination and degradation of Pt *via* our transfer process.[38]

For a wide variety of applications proposed for graphene, the main obstacle has been the absence of a completer transfer method for large-scale graphene films formed on a patterned substrate including insulator regions or voids,[9,39] as shown in Figure 5a. The electric bubbling transfer method was reported to transfer graphene grown on continuous Pt surfaces; however, this process often resulted in the lacerated and/or folded graphene films after the transfer of graphene grown on patterned Pt surfaces, as shown in Figure 5b. We find that the H_2 bubbles were not formed on the discontinuous SiO_2 patterns and the delamination of graphene inhomogeneously occurred at the graphene/Pt interface. However, we could have completely transferred the material without any defects formation such as wrinkles/ripples, tears or folds by introducing the thermal-assisted transfer process, as shown in Figure 5c. During the thermal-assisted transfer, the reaction between Si and Na^+ took place in the boiled NaOH solution to release the PMMA/graphene layer from the SiO_2 surface.[40] The chemical reactions can be represented as follows:

$$SiO_2(s) + 2NaOH(l) \rightarrow Na_2SiO_3(s) + H_2O(l)$$

We suggest that a very thin layer of SiO_2, about a few nanometer thick, was partially etched but enough to release the PMMA/graphene layer. As a result, a homogeneous delamination of graphene from patterned Pt surfaces can be achieved after finite times over 30 min. The transferred films were identified as wrinkles/ripples-free, monolayer graphene based on the OM and Raman spectroscopy (Figure 5c). The associated D and G/2D band maps in Figure 5d demonstrate that the patterned graphene sheet can be completely transferred without further defects formation by introducing the thermal-assisted transfer technique. In addition, it is noted that the underlying, patterned Pt substrates can be reused repeatedly without any additional postprocesses and the graphene obtained from the reused substrate up to three times has almost the same quality as that obtained originally (Supporting Informarion Figure S3).

CONCLUSIONS

In summary, we have demonstrated the controlled growth of wrinkle-free, strictly uniform monolayer graphene films on Pt surfaces with giant grains. We can improve the surface perfectness and limit the number of GB of Pt by texture-controlled giant grain growth, which suppress the undesirable, inhomogeneous C precipitation, enabling us to grow well-crystallized, homogeneous monolayer graphene films. We have developed the thermal-assisted transfer technique for graphene grown on Pt. Our technique has a high tolerance to variations in types and morphologies of underlying substrates during transfer process. Moreover, the transfer technique allows the complete transfer of large-scale patterned graphene films onto arbitrary substrates without any wrinkles/ripples formation, applicable to direct device fabrication without any damage to graphene layer and production of

metal residue on graphene (Supporting Information Figure S4). We believe that our controlled growth and transfer methods are applicable to various kinds of graphene-based device fabrication.

EXPERIMENTAL SECTION

Graphene Synthesis. Graphene was grown on 400 nm-thick Pt films with giant grains using a low-pressure CVD (LP-CVD) system. First, a GGPt (200) or (220) film with a size of ~1 × 1 cm^2 was loaded into a quartz tube in LP-CVD and the quartz tube was elevated up to the process temperature of $T \sim 975$ °C over 40 min with a constant flow of 1 sccm H_2. After reaching $T \sim 975$ °C, a gas mixture of CH_4(5 sccm)/H_2(50 sccm) was introduced into the LP-CVD system for $t = 10$ min to form graphene. Following the growth, the quartz tube was cooled to ~700 °C without changing the gas flow and then finally cooled down to room temperature under vacuum naturally.

Thermal-Assisted Transfer Method. For the transfer of graphene grown on GGPt films, the surface of the graphene was spin-coated with PMMA (Scientific Polymer, 75 000 GPC molecular weight, 10 wt % in toluene) at 4000 rpm for 1 min. In this step, it was highly efficient to reduce the process time that each side of graphene/GGPt film was blocked by Kapton tape. After removing the tape, the PMMA/graphene/GGPt assembly was cured at ~135 °C for 10 min on a hot plate. Next, the PMMA/graphene/GGPt assembly was floated on an aqueous solution of NaOH at temperatures ranging from 25 to 90 °C. The time to completely detach the PMMA/graphene layer from GGPt films depended on the molarity of NaOH solutions and the temperature. Typically, the PMMA/graphene can be perfectly separated within 60 min using a 1 M NaOH aqueous solution at 90 °C. After separation, the PMMA/graphene layers were rinsed in DI water for 30 min and were transferred to SiO_2/Si substrates. Then the sample was dried on a hot plate at 40 °C for 30 min, and baked at 105 °C for 10 min to strongly adhere to SiO_2/Si substrates. Finally, the PMMA was removed using acetone, leaving behind a graphene film on SiO_2/Si substrates.

Characterization. As-grown GGPt films were analyzed by an AFM (Veeco Multimode V) to observe surface morphologies. The AFM was operated using tapping mode to acquire a scan size of 2 × 2 μm^2. The surface morphologies of the graphene/GGPt films and transferred graphene on SiO_2 substrates were observed using a FE-SEM (FEI Nanonova 230) at an acceleration voltage of 10 to 20 kV. An orientation mapping was accomplished by obtaining EBSD in the FE-SEM. The crystallographic orientations of the GGPt films were analyzed by XRD pattern by using an X-ray diffractometer (Bruker D8 Advance) using Cu−Kα as the X-ray source (λ: 5046 Å). The presence and chemical states of foreign species in the GGPt films were studied using XPS (Thermo Fisher). The XPS studies were conducted on a K-α spectrometer using Al K-α nonmonochromatic X-ray excitation at a power of 72 W, with an analysis area diameter of ~10 mm and a pass energy of 50 eV for the electron analysis. The base pressure of the analysis chamber was below ~1 × 10^{-9} mbar. The Pt−O compositions in the GGPt films were investigated by dividing the individual peak areas. Successfully transferred graphene layers were confirmed by Raman spectroscopy. Both the Raman spectra and mappings were obtained from a graphene layer which was transferred onto a 300 nm-thick SiO_2/Si. The Raman spectroscopy and mapping were carried out on a WiTec alpha 300R M-Raman system with a 532 nm excitation wavelength (2.33 eV). A laser spot had a dimension of ~640 nm for a ×50 objective lens with numerical aperture of 0.5 and the laser power was ~2 mW. The Raman spectra were analyzed and the Raman images were collected by a computer-controlled x-y translation stage with a raster scan. Spectroscopic mapping images were created by measuring the Raman spectra of each individual pixel with a 50 × 50 μm^2 step size using a WiTec Project software. The Raman data mentioned in this manuscript, such as the FWHM values and intensity ratio of the G-to-2D bands were arithmetical averages of values that were measured at more than 30 different points per sample. The graphene layers were transferred onto carbon holey coated Au TEM grids by utilizing direct transfer method. Next, the TEM images of wrinkle-free graphene sheets were obtained using a JEOL 2100F (installed at Korea Institute of Materials Science) that operated at 200 kV which was equipped with a Gatan image filter system. The Gatan Digital Micrograph software was used for the image processing and analysis. Electrical characterizations of the graphene layers were analyzed by fabricating a FET device. Bottom-gated FET devices were fabricated by transferring the graphene layers onto p-Si substrates with 300 nm thick thermal oxide. Conventional photolithography and the O_2 plasma-etching process were applied to acquire FET devices with a channel widths of 100 μm and channel length of 200 μm. Source-drain electrodes (Cr/Au: 10 nm/60 nm) were deposited using an e-beam evaporator. The electrical measurement was obtained by standard 4-probes station (MS-tech, Agilent Technologies B1500A) at room-temperature. From the plot of the source-drain current as a function of gate voltage from −20 to +100 V, we extracted carrier mobility values from the slope.

Conflict of Interest: The authors declare no competing financial interest.

Supporting Information Available: (Figure S1) Atomic models of graphene on Pt surfaces with different preferred orientations. (Figure S2) Surface morphologies of as-synthesized graphene on a Cu foil and GGPt substrates and transferred graphene onto a SiO_2 surface. (Figure S3) Growth of wrinkle-free graphene on a reused, patterned Pt substrate. (Figure S4) Complete transfer of graphene grown on a patterned GGPt substrate using the thermal-assisted transfer technique. This material is available free of charge via the Internet at http://pubs.acs.org.

Acknowledgment. We gratefully acknowledge supports from the National Research Foundation (NRF) funded by the Korean government through the Bio and Medical Technology Development Program (Grant No. NRF-2012M3A9C6049797) and through the Midcareer Researcher Program (Grant No. NRF-2013R1A2A2A04015946) and through the Basic Science Research Program (Grant No. 2011-0014807) and through the National Nuclear R&D program (Grant No. 2014M2B2A-9031944). S.-Y.K. and H.-J.S. planned and supervised the project; J.-K.C. and J.K. performed the experiments, with assistances from S.-D.P., H.D.Y, S.-Y. Kim, M.J. and J.-K.C., J.K., S.Y.K., S.K., H.-J.S. and S.-Y.K. analyzed the data; S.-D.K. performed TEM measurements of the samples; J.-K.C. and K.P. performed the electrical measurements; D.-Y.P., D.-S.L. and S.-K.H. performed the growth experiments of texture-controlled platinum films with giant grains, with assistance from a technical team of GMEK incorporation; S.-Y.K., J.-K.C. and H.-J.S. wrote the manuscript.

REFERENCES AND NOTES

1. Novoselov, K. S.; Geim, A. K.; Morozov, S. V.; Jiang, D.; Zhang, Y.; Dubonos, S. V.; Grigorieva, I. V.; Firsov, A. A. Electric Field Effect in Atomically Thin Carbon Films. *Science* **2004**, *306*, 666–669.
2. Bolotin, K. I.; Sikes, K. J.; Jiang, Z.; Klima, M.; Fudenberg, G.; Hone, J.; Kim, P.; Stormer, H. L. Ultrahigh Electron Mobility in Suspended Graphene. *Solid State Commun.* **2008**, *146*, 351–355.
3. Balandin, A. A.; Ghosh, S.; Bao, W.; Calizo, I.; Teweldebrhan, D.; Miao, F.; Lau, C. N. Superior Thermal Conductivity of Single-Layer Graphene. *Nano Lett.* **2008**, *8*, 902–907.
4. Kwon, S.-Y.; Ciobanu, C. V.; Petrova, V.; Shenoy, V. B.; Bareno, J.; Gambin, V.; Petrov, I.; Kodambaka, S. Growth of Semiconducting Graphene on Palladium. *Nano Lett.* **2009**, *9*, 3985–3990.

5. Berger, C.; Song, Z.; Li, X.; Wu, X.; Brown, N.; Naud, C.; Mayou, D.; Li, T.; Hass, J.; Marchenkov, A. N.; *et al.* Electronic Confinement and Coherence in Patterned Epitaxial Graphene. *Science* **2006**, *312*, 1191–1196.
6. Strupinski, W.; Grodecki, K.; Wysmolek, A.; Stepniewski, R.; Szkopek, T.; Gaskell, P. E.; Gruneis, A.; Haberer, D.; Bozek, R.; Krupka, J.; Baranowski, J. M. Graphene Epitaxy by Chemical Vapor Deposition on SiC. *Nano Lett.* **2011**, *11*, 1786–1791.
7. Sun, Z.; Yan, Z.; Yao, J.; Beitler, E.; Zhu, Y.; Tour, J. M. Growth of Graphene from Solid Carbon Sources. *Nature* **2010**, *468*, 549–552.
8. Kwak, J.; Chu, J. H.; Choi, J.-K.; Park, S.-D.; Go, H.; Kim, S. Y.; Park, K.; Kim, S.-D.; Kim, Y.-W.; Yoon, E.; Kodambaka, S.; Kwon, S.-Y. Near Room-Temperature Synthesis of Transfer-Free Graphene Films. *Nature Commun.* **2012**, *3*, 645.
9. Reina, A.; Jia, X.; Ho, J.; Nezich, D.; Son, H.; Bulovic, V.; Dresselhaus, M. S.; Kong, J. Large Area, Few-Layer Graphene Films on Arbitrary Substrates by Chemical Vapor Deposition. *Nano Lett.* **2008**, *9*, 30–35.
10. Li, X.; Cai, W.; An, J.; Kim, S.; Nah, J.; Yang, D.; Piner, R.; Velamakanni, A.; Jung, I.; Tutuc, E.; Banerjee, S. K.; *et al.* Large-Area Synthesis of High-Quality and Uniform Graphene Films on Copper Foils. *Science* **2009**, *324*, 1312–1314.
11. Dai, B.; Fu, L.; Zou, Z.; Wang, M.; Xu, H.; Wang, S.; Liu, Z. Rational Design of a Binary Metal Alloy for Chemical Vapour Deposition Growth of Uniform Single-Layer Graphene. *Nat. Commun.* **2011**, *2*, 522.
12. Wu, Y. A.; Fan, Y.; Speller, S.; Creeth, G. L.; Sadowski, J. T.; He, K.; Robertson, A. W.; Allen, C. S.; Warner, J. H. Large Single Crystals of Graphene on Melted Copper Using Chemical Vapor Deposition. *ACS Nano* **2012**, *6*, 5010–5017.
13. Liu, W.; Li, H.; Xu, C.; Khatami, Y.; Banerjee, K. Synthesis of High-Quality Monolayer and Bilayer Graphene on Copper Using Chemical Vapor Deposition. *Carbon* **2011**, *49*, 4122–4130.
14. Li, X.; Magnuson, C. W.; Venugopal, A.; An, J.; Suk, J. W.; Han, B.; Borysiak, M.; Cai, W.; Velamakanni, A.; Zhu, Y.; Fu, L.; *et al.* Graphene Films with Large Domain Size by a Two-Step Chemical Vapor Deposition Process. *Nano Lett.* **2010**, *10*, 4328–4334.
15. Li, X.; Magnuson, C. W.; Venugopal, A.; Tromp, R. M.; Hannon, J. B.; Vogel, E. M.; Colombo, L.; Ruoff, R. S. Large-Area Graphene Single Crystals Grown by Low-Pressure Chemical Vapor Deposition of Methane on Copper. *J. Am. Chem. Soc.* **2011**, *133*, 2816–2819.
16. Yu, Q.; Jauregui, L. A.; Wu, W.; Colby, R.; Tian, J.; Su, Z.; Cao, H.; Liu, Z.; Pandey, D.; Wei, D.; Chung, T. F.; *et al.* Control and Characterization of Individual Grains and Grain Boundaries in Graphene Grown by Chemical Vapour Deposition. *Nat. Mater.* **2011**, *10*, 443–449.
17. Banhart, F.; Kotakoski, J.; Krasheninnikov, A. V. Structural Defects in Graphene. *ACS Nano* **2010**, *5*, 26–41.
18. Gao, J. H.; Sagisaka, K.; Kitahara, M.; Xu, M. S.; Miyamoto, S.; Fujita, D. Graphene Growth on a Pt(111) Substrate by Surface Segregation and Precipitation. *Nanotechnology* **2012**, *23*, 055704.
19. Sutter, P.; Sadowski, J. T.; Sutter, E. Graphene on Pt(111): Growth and Substrate Interaction. *Phys. Rev. B* **2009**, *80*, 245411.
20. Yoon, D.; Son, Y. W.; Cheong, H. Negative Thermal Expansion Coefficient of Graphene Measured by Raman Spectroscopy. *Nano Lett.* **2011**, *11*, 3227–3231.
21. Mattevi, C.; Kim, H.; Chhowalla, M. A Review of Chemical Vapour Deposition of Graphene on Copper. *J. Mater. Chem.* **2011**, *21*, 3324.
22. Gao, L.; Guest, J. R.; Guisinger, N. P. Epitaxial Graphene on Cu(111). *Nano Lett.* **2010**, *10*, 3512–3516.
23. Lahiri, J.; S Miller, T.; J Ross, A.; Adamska, L.; Oleynik, I. I.; Batzill, M. Graphene Growth and Stability at Nickel Surfaces. *New J. Phys.* **2011**, *13*, 025001.
24. Yu, Q.; Lian, J.; Siriponglert, S.; Li, H.; Chen, Y. P.; Pei, S.-S. Graphene Segregated on Ni Surfaces and Transferred to Insulators. *Appl. Phys. Lett.* **2008**, *93*, 113103.
25. Baker, H.*et al.*; Alloy Phase Diagrams. In *ASM Handbook*; ASM International: 2002; Vol. 3.
26. Wang, Y.; Zheng, Y.; Xu, X.; Dubuisson, E.; Bao, Q.; Lu, J.; Loh, K. P. Electrochemical Delamination of CVD-Grown Graphene Film: Toward the Recyclable Use of Copper Catalyst. *ACS Nano* **2011**, *5*, 9927–9933.
27. Gao, L.; Ren, W.; Xu, H.; Jin, L.; Wang, Z.; Ma, T.; Ma, L. P.; Zhang, Z.; Fu, Q.; Peng, L. M.; *et al.* Repeated Growth and Bubbling Transfer of Graphene with Millimetre-Size Single-Crystal Grains Using Platinum. *Nat.ommun.* **2012**, *3*, 699.
28. Chu, J. H.; Kwak, J.; Kwon, T.-Y.; Park, S.-D.; Go, H.; Kim, S. Y.; Park, K.; Kang, S.; Kwon, S.-Y. Facile Synthesis of Few-Layer Graphene with a Controllable Thickness Using Rapid Thermal annealing. *ACS Appl. Mater. Interfaces* **2012**, *4*, 1777–1782.
29. Kim, M. H.; Park, T.-S.; Lee, D.-S.; Yoon, E.; Park, D.-Y.; Woo, H.-J.; Chun, D.-I.; Ha, J. Highly (200)-Oriented Pt Films on SiO_2/Si Substrates by Seed Selection through Amorphization and Controlled Grain Growth. *J. Mater. Res.* **1999**, *14*, 634–637.
30. Saenger, K. L.; Rossnagel, S. M. Properties and Decomposition Behaviors of Reactively Sputtered Pt(O) Electrode Materials. *Mater. Res. Soc. Symp. Proc.* **2000**, *596*, 57–65.
31. Lee, D.-S.; Park, D.-Y.; Woo, H.-J.; Kim, S.-H.; Ha, J.; Yoon, E. Preferred Orientation Controlled Giant Grain Growth of Platinum Thin Films on SiO_2/Si Substrates. *Jpn. J. Appl. Phys.* **2001**, *40*, L1.
32. Hecq, M.; Hecq, A. Oxygen Induced Preferred Orientation of DC Sputtered Platinum. *J. Vac. Sci. Technol.* **1981**, *18*, 219–222.
33. Thompson, C. V.; Carel, R. Texture Development in Polycrystalline Thin Films. *Mater. Sci. Eng., B* **1995**, *32*, 211–219.
34. Körber, C.; Suffner, J.; Klein, A. Surface Energy Controlled Preferential Orientation of Thin Films. *J. Phys. D: Appl. Phys.* **2010**, *43*, 055301.
35. Francis, A. J.; Salvadora, P. A. Crystal Orientation and Surface Morphology of fcc Metal Thin Films Deposited upon Single Crystal Ceramic Substrates Using Pulsed Laser Deposition. *J. Mater. Res.* **2007**, *22*, 89–102.
36. Anantatmula, R.; Pitman, S.; Lund, A. *Selection of Replacement Material for the Failed Surface Level Gauge Wire in Hanford Waste Tanks*; Westinghouse Hanford Co., Richland, WA. Funding Organisation: USDOE, Washington, DC (United States): 1995.
37. Azaroual, M.; Romand, B.; Freyssinet, P.; Disnar, J.-R. Solubility of Platinum in Aqueous Solutions at 25 °C and pHs 4 to 10 under Oxidizing Conditions. *Geochim. Cosmochim. Acta* **2001**, *65*, 4453–4466.
38. Parkinson, C. R.; Walker, M.; McConville, C. F. Reaction of Atomic Oxygen with a Pt(111) Surface: Chemical and Structural Determination Using XPS, CAICISS and LEED. *Surf. Sci.* **2003**, *545*, 19–33.
39. Geim, A. K.; Novoselov, K. S. The Rise of Graphene. *Nat. Mater.* **2007**, *6*, 183–191.
40. Reina, A.; Son, H.; Jiao, L.; Fan, B.; Dresselhaus, M. S.; Liu, Z.; Kong, J. Transferring and Identification of Single-and Few-Layer Graphene on Arbitrary Substrates. *J. Phys. Chem. C* **2008**, *112*, 17741–17744.